Probabilistic Modelling of the Conceptual Design Phase in Automotive Engineering

Charbel Mallah[a], Christoph David [b], Marko Alder[c]

[a] *German Aerospace Center, Institute of Vehicle Concepts, Pfaffenwaldring 38-40, 70569 Stuttgart, Germany, Charbel.Mallah@dlr.de*
[b] *German Aerospace Center, Institute of Vehicle Concepts, Pfaffenwaldring 38-40, 70569 Stuttgart, Germany, Christoph.David@dlr.de*
[c] *German Aerospace Center, Institute of System Architectures in Aeronautics, Hein-Sass-Weg 22, 21129 Hamburg Germany, Marko.Alder@dlr.de*

Abstract

The multidisciplinary nature of the vehicle design process and the increasing demand for developing environmentally sustainable transport systems present a challenge to the automotive industry. These challenges are associated with uncertainties that are often neglected in the conceptual design phase of road vehicles. To address such uncertainties, a probabilistic approach can be adopted. More precisely, one can make use of the so called Sobol' indices. These are used within the context of variance-based global sensitivity analysis to quantify the uncertainties of a system's outputs caused by the uncertainties of its inputs. For this purpose, this paper aims to achieve the following goals:

1. Quantification of output uncertainties in the conceptual design phase based on the Sobol' indices. Within this context, the research plug-in hybrid electric vehicle "Interurban Vehicle" (IUV), designed at the German Aerospace Centre (DLR[1]), is considered.

2. Probabilistic, digital and parametric modelling of the IUV based on multidisciplinary design analysis (MDA).

Overall, this paper concludes that probabilistic modelling does not only enable the quantification of uncertainties, but also helps to understand the underlying complex mechanisms of the considered system and support the decision-making process in the conceptual design phase of road vehicles.

Keywords: uncertainty quantification, Sobol' indices, plug-in hybrid electric vehicle, conceptual design phase, automation, digitization, multidisciplinary design analysis (MDA)

1. Introduction

1.1. Problem setting

Nowadays, the world is witnessing an exponential growth in technological advances that are revolutionizing almost every major industry. As a result, the complexity of products is increasing to a large extent. Road vehicles serve as a good example of this transformation. During the last couple of decades, vehicles evolved from being mainly a mechanical product to an increasingly interconnected system involving heterogeneous stakeholders as well as multidisciplinary requirements and constraints. In addition to this increasing complexity of the vehicle architectures, the pursuit of developing environmentally and economically sustainable transport systems as well as the resulting regulatory changes present a common challenge to the automotive industry. To address these challenges, important

[1] DLR: Deutsches Zentrum für Luft- und Raumfahrt

decisions should be made in the early phase of the vehicle design, also known as the concept phase or conceptual design phase. This phase is crucial, as it establishes the core design, performance criteria and the majority of the costs during the later stages. Therefore, it is essential to pinpoint the design factors, such as material parameters, operational conditions, etc., that have the greatest impact on the final design [18]. However, such factors are subjected to uncertainties that are often neglected in the conceptual design phase. In general, there are two distinct types of uncertainties, namely aleatory and epistemic [9]. On one hand, aleatory uncertainties arise from the intrinsic randomness of the system or process considered, like, for instance, the variability of material properties in manufacturing processes. Such uncertainties cannot be reduced by acquiring additional information or improving models. On the other hand, epistemic uncertainties stem from a lack of information or data and can be reduced by obtaining additional information or improving models [13]. Moreover, Kennedy and O'Hagan, 2001 [16] classified uncertainties in a more precise manner. They identified six types of uncertainties [15]: 1) parametric variability, 2) parameter uncertainty, 3) model inadequacy, 4) interpolation uncertainty, 5) numerical uncertainty and 6) experimental variability. Within the scope of this publication, emphasis is placed on uncertainties of the vehicle design parameters, i.e., parametric variability[2] and parametric uncertainty[3]. Efficiency of vehicle components and gravimetric energy densities serve as good examples for such vehicle design parameters. Accounting for such uncertainties in the conceptual design phase requires a shift from deterministic designing to a probabilistic one. In contrast to deterministic approaches, probabilistic ones can be utilized to analyze various design scenarios. Consequently, this enhances the robustness of the design concept by ensuring that it fulfills the requirements under a variety of conditions [22]. Furthermore, by analyzing different scenarios vehicle designers can extrapolate from current technological trends to create designs that incorporate possible future advancements. However, the interdisciplinary nature of the conceptual design phase, as well as the complex interconnections between the various engineering disciplines involved, render the integration of a probabilistic framework challenging.

1.2. State of the art and research gap

Within this context, sensitivity analysis (SA) can play a crucial role in accounting for uncertainties of the vehicle design parameters and thus establish a probabilistic framework for the conceptual design phase. In general, SA is referred to as the study that examines how the outputs of a system are connected to, and affected by the inputs of that system [25]. I.e., SA techniques quantify the impact of the input parameters on the outputs of the considered system. There are various ways how to conduct SA. Broadly speaking, methods of SA can be categorized into two main groups [33]:

1. **Local SA** (LSA) examines the local impact of a single input parameter on the system's output by varying the considered input parameter and fixing the remaining input parameters at a specific operating or design point. Such methods do not assign probability distributions to the input parameters [28]. The "one-factor-at-a-time" technique serves as a good example for such local approaches.

2. **Global SA** (GSA) asses the sensitivity of the system's output with respect to the variation of the entire input parameter space, rather than taking only a single design point into consideration as was the case using LSA.

To clarify the difference between LSA and GSA, the simulation of a vehicle's energy consumption is considered. The energy consumption depends on some input parameters, such as a specific driving cycle, vehicle's mass, aerodynamic drag coefficient, etc. Conducting an LSA, one might examine how small variations in, for instance the vehicle's mass affect the vehicle's energy consumption, while holding the remaining inputs constant. On the other hand, a GSA involves varying each input parameter across its entire plausible range and measuring how much each parameter impacts the vehicle's energy consumption. Therefore, GSA plays an important role in determining which parameters have the greatest impact and which ones should remain unchanged. For this reason, GSA techniques are suitable for

[2] Parametric variability points to the variation in the design variables and/or noise variables [15].
[3] Parameter uncertainty is related to fixed and non-measurable parameters of a simulation model (e.g. fracture coefficient) [15].

the initial design phase, since in the early design phases, it is often challenging to determine which parameters exert the greatest influence and which should remain constant [18]. However, there is not a unique way to conduct GSA. Razavi et al., 2021 [25] categorize GSA into five main groups: 1) derivative-based approach, 2) distribution-based approach, 3) variogram-based approach, 4) regression-based approach and 5) response surface-assisted GSA.
Within the scope of this paper only the distribution-based approach is considered. Distribution-based GSA examines the distributional properties of the output. Most commonly, distribution-based GSA involves partitioning the variance of the output into portions which are then attributed to the corresponding inputs [12, 18]. This assumes that the variance is a reliable measure of uncertainty. Such approaches are also known as "variance-based GSA". One of their key characteristics is their independence from the considered model or system. That is, conducting the analysis does not depend on the model's characteristics (linear, nonlinear, stationary, etc.) [28]. Typical representative of distribution-based GSA or variance-based GSA is the Sobol' method [31]. For a more comprehensive literature review regarding SA, it is referred to Razavi et al., 2021 [25].

To address the challenging task of incorporating uncertainties in the vehicle design process, several attempts were made, especially within the context of vehicle dynamics simulations.

In the work of Song et al., 2023 [32], SA was conducted on the input parameters of a nonlinear five-degree-of-freedom seated human model [2]. The main objective was to quantify the output uncertainties of the ride comfort with respect to the input uncertainties of the model's stiffness parameters. Here, the input uncertainties were quantified by assigning probability density functions (PDFs) to the input stiffness parameters. Within this context, Song et al., adopted a local approach for the SA. Each uncertain input parameter was varied separately, while keeping the other uncertain inputs constant. Subsequently, polynomial chaos expansion (PCE) [36] was used as a surrogate model to efficiently compute the output of the human model, i.e., the ride comfort, and characterize its uncertainties.

Brandt et al., 2022 [6] analyzed the crosswind stability of a vehicle by examining various crosswind gust profiles. For this purpose, Brandt et al., integrated vehicle dynamics models, such as the single-track model [30], with aerodynamic ones following a one-way-coupling approach. Here, uncertainties of input parameters from both disciplines (vehicle dynamics and aerodynamics), such as wheel-base, vehicle mass and lift coefficients were considered. Within this context, the input uncertainties were quantified using parameter intervals chosen based on existing vehicle specifications as well as vehicle types. To quantify the output uncertainties of the vehicle's crosswind stability, the main effect of the inputs on the crosswind stability was computed, i.e., how each input affects the output. Moreover, the effect of the inputs' interactions on the output was also studied based on response surface methodology (RSM) [5], which aims at developing a mathematical model based on statistical techniques.

Danquah et al., 2021 [8] examined the uncertainties of the energy consumption of an electric vehicle based on the Worldwide Harmonized Light Vehicle Test Procedure (WLTP). In order to compute the energy consumption, an open-source vehicle dynamics simulation was used, which can be found in [7]. PDFs as well as intervals were assigned to the input parameters, such as the vehicle mass, aerodynamic drag coefficient, tire pressure, etc., to quantify their uncertainties. Based on these intervals and PDFs, the simulation was performed repeatedly to quantify the uncertainties of the energy consumption stemming from the input uncertainties. Moreover, the simulated energy consumption was validated by experimental measurements, in which a prototype vehicle was placed on a chassis dynamometer. Subsequently, the error between the simulated and experimental energy consumption was computed, with the objective of quantifying the uncertainties of the simulation model used.

Schmeiler et al., 2016 [28] made use of various techniques to conduct SA on input parameters of vehicle dynamics simulations. More precisely, three simulations were considered. Two of them are based on the single-track model, which examines the lateral dynamics of a road vehicle. The third simulation is based on a commercial high-fidelity black-box model. The sensitivity of the yaw rate, roll angle and rollover risk were analyzed with respect to simulation input parameters such as mass, inertia, position of center of gravity, cornering stiffness, etc. For this purpose, distribution-based GSA, represented by the Sobol' method [31] as well as surface-assisted GSA, represented by PCE were used. Moreover, regionalized SA (RSA) was applied, which can be linked to GSA approaches. The main

objective of RSA is to set a condition on the output space (for instance, an upper limit) and categorize the outputs that satisfy this condition as behavioral, otherwise as non-behavioral [24].

Wu et al., 2015 [37], analyzed the uncertainties of simulation input parameters within the context of vehicle vertical dynamics. To be more precise, a four-degree-of-freedom vehicle roll dynamics model was considered. Here, Wu et al. quantified input uncertainties by assigning PDFs to the suspension's stiffness parameters. Moreover, an approach was proposed to also considered parameter intervals, as it is sometimes challenging to determine the PDF of certain input parameters, such as the vehicle's payload capacity. Within this context, surface-assisted GSA, represented by PCE combined with interval analysis [21] were implemented to characterize the output uncertainty of the suspension's deformation.

Within the context of road vehicles, SA techniques are well-established and have been extensively studied. However, to the author's knowledge, their usage is limited to specific vehicle dynamics models, rather than considering the whole conceptual phase of road vehicles. For this reason, this paper aims on answering the following research questions:

- *How can a probabilistic approach be adopted with the objective of quantifying uncertainties in the multidisciplinary conceptual design phase of road vehicles?*

- *How can the collaboration regarding computational tools across the engineering teams involved in the multidisciplinary conceptual design phase of road vehicles be enhanced?*

1.3. Contribution and outline

With the objective of answering the research questions stated above, this paper aims at providing a framework that incorporates a probabilistic approach in the conceptual design phase of road vehicles. Specifically, it employs the so called Sobol' indices (see Chapter 2) used within the context of variance-based GSA in order to:

- quantify the uncertainties of the outputs of interest, which are caused by the uncertainties of the considered design parameters reflecting possible technological improvements,

- identify the most influential design factors on the final vehicle concept and

- help in understanding the underlying mechanisms and interactions between the design factors governing the behavior of the vehicle concept.

As a result, the decision-making process in the conceptual phase is enhanced. With aim of digitizing and automating the conceptual design phase and improving the exchange of computational tools across the distinct engineering teams involved, a digital design workflow is built using the **m**ultidisciplinary **d**esign **a**nalysis and **o**ptimization (MDAO) workflow design accelerator (MDAx) and is then executed in the process integrating open-source software RCE, short for **r**emote **c**omponent **e**nvironment (see Chapter 3). In order to show that this approach is applicable to the state-of-the-art vehicle concepts, the conceptual design phase of the research vehicle "Interurban Vehicle" (IUV) is considered (see Chapter 4). The IUV is a plug-in fuel cell electric vehicle conceptualized at the German Aerospace Centre (DLR[4]) in Stuttgart, Germany. To reduce the complexity of the problem at hand, the IUV's design workflow was reduced to include the following disciplines: vehicle performance, engine, fuel cell, energy storage, mission, mass, operating costs and well-to-wheel processes. Finally, the results of the IUV's probabilistic conceptual design phase with regard

[4] DLR: Deutsches Zentrum für Luft- und Raumfahrt

to the Sobol' indices are discussed and the impact of the design factors on the vehicle concept as well as their interactions are analyzed (see Chapter 5).

2. Fundamentals of GSA

In contrast to deterministic approaches, in a probabilistic framework, inputs and outputs are regarded as random variables [10]. Let $f\colon \mathbb{R}^d \mapsto \mathbb{R}$ be a computational model such that:

$$Y = f(\boldsymbol{X}). \tag{1}$$

Here, $Y \in \mathbb{R}$ represents a scalar uncertain output with an unknown PDF and $\boldsymbol{X} = [X_1, X_2, \cdots, X_d]^{\mathrm{T}} \in \mathbb{R}^d$ denotes the random vector of $d \in \mathbb{N}_{>0}$ uncertain input parameters. Each input parameter X_i for $i \in \{1,2,\cdots,d\}$ is assigned a known PDF to reflect the uncertainties, to which it is subjected. The main objective of GSA is to assess the uncertainty of the output Y with respect to the variation of the input parameters $\boldsymbol{X}$.

2.1. Variance-based GSA

Variance-based GSA assumes that the variance is a reliable indicator of uncertainty. For this reason, $f(\boldsymbol{X})$ is decomposed into finite orthogonal components based on the high dimensional model representation (HDMR) technique (see [31] for further details). Subsequently, applying the law of variance and under the assumption that the uncertain input parameters $\boldsymbol{X} = [X_1, X_2, \cdots, X_d]^{\mathrm{T}}$ are independent, the output variance $\mathbb{V}[\mathrm{Y}]$ is written as:

$$\mathbb{V}[Y] = \sum_{i=1}^{d} \mathbb{V}\big[\mathbb{E}[Y|X_i]\big] + \sum_{1\le i<j\le d} W_{i,j} + \cdots + W_{i,j,\ldots,d}\,, \tag{2}$$

where

$$W_{i,j} = \mathbb{V}\Big[\mathbb{E}\big[Y\big|X_{i,j}\big]\Big] - \mathbb{V}\big[\mathbb{E}[Y|X_i]\big] - \mathbb{V}\Big[\mathbb{E}\big[Y\big|X_j\big]\Big]. \tag{3}$$

Here, $\mathbb{V}[\cdot]$ and $\mathbb{E}[\cdot]$ denote the variance and the expected value operators, respectively. The contributions of the input parameters $\boldsymbol{X}$ to the uncertainty of the output Y is then quantified using the sensitivity measures, also known as the Sobol' indices. These are acquired by dividing both sides of Eq. 2 by $\mathbb{V}[\mathrm{Y}]$. Here, three major Sobol' indices are defined:

1. The first-order Sobol' index S_i measures the main effect of an input parameter X_i on the output uncertainty and is described as follows:

$$S_i = \frac{\mathbb{V}\big[\mathbb{E}[Y|X_i]\big]}{\mathbb{V}[Y]}. \tag{4}$$

2. The second-order Sobol' index $S_{i,j}$ measures the interaction effect between the i-th and j-th input parameter, X_i and X_j $(i, j \in \{1,2,\cdots,d\})$, on the output uncertainty and is described by:

$$S_{i,j} = \frac{\mathbb{V}\Big[\mathbb{E}\big[Y\big|X_{i,j}\big]\Big]}{\mathbb{V}[Y]}. \tag{5}$$

3. The total Sobol' index S_{Ti} measures the main effect of X_i as well as its interaction effect with the other input parameters $\boldsymbol{X}_{\sim i}$. Here, $\sim i$ denotes the indices of all input parameters except the index i. S_{Ti} is defined as follows:

$$S_{Ti} = 1 - \frac{\mathbb{V}\big[\mathbb{E}[Y|\boldsymbol{X}_{\sim i}]\big]}{\mathbb{V}[Y]} = S_i + \sum_{j=1, j\neq i}^{d} S_{i,j} + \cdots + S_{i,j,\ldots,d} \tag{6}$$

From Eq. 6, one can deduce that the difference $S_{Ti} - S_i$ is an indicator for the interaction effect of the i-th input parameter with the remaining input parameters on the output uncertainty.

2.2. Numerical approximation of variance-based GSA

The calculation of the Sobol' indices based on Eq. 4, 5 und 6 requires solving multiple integrals stemming from the variance $\mathbb{V}[\cdot]$ and expected value $\mathbb{E}[\cdot]$ operators. This is only possible if an analytical function is given to compute the output Y. Even in this case, solving such multiple integrals can be an exhausting task. As a remedy, one can make use of sampling-based approaches, more precisely, Monte-Carlo methods to estimate the value of multiple integrals. Within the scope of this paper, only one Monte-Carlo based approach is considered, namely the Sobol' method [31]. More precisely, the implementation of this approach in the Python library SALib [14] is used. Here, there are three main steps (see Figure 1)

i. The input parameters are randomly sampled based on the PDFs assigned to them. To reduce clustering and gaps in the input parameter space, low-discrepancy sequences such as the Sobol' sequence are used for sampling. In this paper, the Saltelli's sampling scheme is considered. It enhances the Sobol' sequence to lower the error rates in the Sobol' index calculations [11, 26].

ii. The model f is evaluated at each sample point.

iii. The Sobol' indices S_i, S_{ij} and S_{Ti} are computed by making use of estimators for $\mathbb{V}[\cdot]$ and $\mathbb{E}[\cdot]$ (see [31] for further details).

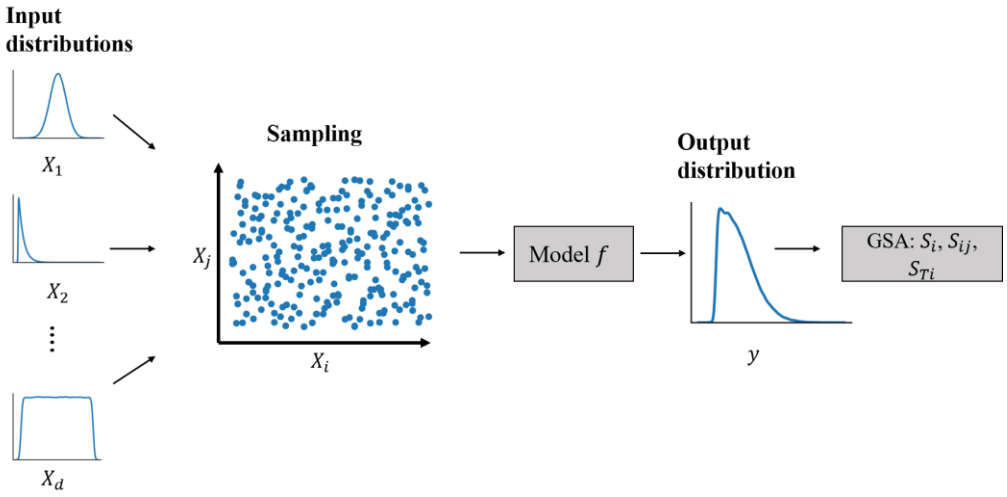

Figure 1: Global sensitivity analysis

3. Multidisciplinary conceptual design phase

Due to the complex system architecture of road vehicles, there are multiple disciplines involved in the conceptual design phase. Each of these disciplines has its own set of computational tools that encapsulate domain-specific expertise. This presents challenges for cross-team collaboration, particularly in the integration of computational tools during the conceptual design phase, and prompts the following question:

- *How can the methodologies and computational tools of the involved disciplines be fused into an integrated design process?*

In order to tackle the above-mentioned problem, a framework is needed that aims at digitizing and automating the conceptual design phase of road vehicles. For this purpose, the framework in figure (2) is considered.

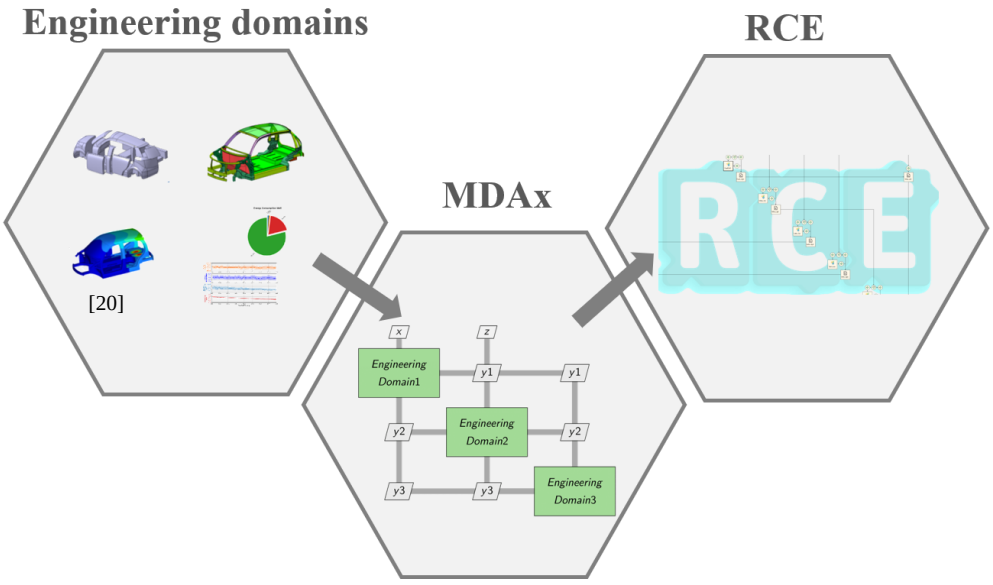

Figure 2: Framework to digitize and automate the conceptual design phase of road vehicles (MDAx: multidisciplinary design analysis and optimization workflow design accelerator RCE: remote component environment)

MDAx to RCE

The framework presented in Figure 2 facilitates the involvement of discipline experts across various locations in the design process [1]. The open-source software **r**emote **c**omponent **e**nvironment (RCE) [4], developed primarily at DLR, serves as a good example for such a process integrating framework. RCE allows designers to build automated workflows consisting of several analysis modules, i.e. computation tools. The workflow is then executed in an automated manner. More precisely, each computational tool, hosted on its respective server, is invoked, and the necessary data is exchanged automatically [4]. However, the process of building such a workflow can become a tedious task, especially if the workflow at hand is a complex one. Even with a complex workflow in place, implementing modifications, verifying tool couplings and ensuring proper tool functionality will remain a time-consuming process. For this purpose, the multidisciplinary design analysis and optimization (MDAO) workflow design accelerator, abbreviated as MDAx, comes into play. To simplify the process of modeling complex engineering workflows, Risueño et al. [23] introduced MDAx in 2020. MDAx is a user-friendly tool, which enables the user to easily build and modify an engineering workflow using drag and drop operations. More precisely, the user can define computational tools and specify the corresponding input and output parameters for each tool. The workflow is then automatically modeled in the form of an extended design structure matrix (XDSM) [17]. Figure 3 illustrates an XDSM representation of a workflow model. The computational tools of the involved disciplines are placed on the XDSM diagonal. The data connection between these tools is represented by the thick gray lines. More precisely, the input parameters of each computational tool are placed on the vertical line connected to this tool, whereas the output parameters are placed on the horizontal line. Additionally, MDAx provides some verification functionalities. To be more precise, it checks if the system requires any parameters before it can provide them and if the same parameters are being provided by more than one tool [23]. Finally, after modeling the workflow, the XDSM can be exported to a process integration software, such as RCE, where the workflow execution is carried out.

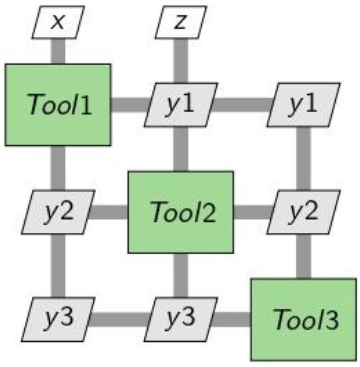

Figure 3: XDSM representation of a workflow model

4. Implementation: interurban vehicle

4.1. Interurban vehicle (IUV)

The Interurban Vehicle (IUV) is a vehicle concept developed within the DLR "Next Generation Car" project. The development of the IUV concept focuses on four key pillars: comfort, performance, safety and sustainability. These four elements define the high-level multidisciplinary requirements of the IUV.
Passenger comfort is addressed by specifications such as driving automation at an automation degree of SAE (Society of Automotive Engineers) level 4, a flexible interior and an ergonomic entrance concept. To ensure an ergonomic entrance, a wide entry way to the vehicle was established by relinquishing the b-pillar from being a fixed part of the IUV's body-in-white. This poses some challenges with respect to the IUV's passive safety. More precisely, the IUV's body-in-white has to be modified to maintain the vehicle's structural integrity despite the missing b-pillar.
In terms of performance, a total driving range of up to 1000km is defined. The challenge of enabling such long ranges for a five-seater vehicle is addressed by using hydrogen and a high voltage battery as energy sources combined with the development of lightweight structures for weight reduction. A zero-emission powertrain is achieved with an electrified driving system extended by a hydrogen-powered fuel-cell system.
Considering the above, there are several design questions that should be addressed in the conceptual design phase. For instance:

- *How should the IUV's powertrain be configured in terms of the energy ratio between the battery and the hydrogen tank, to meet the required driving range?*

- *Which material and structural concept should be adopted for the IUV's body-in-white such that the multidisciplinary requirements, sustainability, performance, safety and comfort standards are met?*

4.2. IUV's design workflow

To answer the above questions, a design workflow is developed. Its objective is to generate a consistent gravimetric and volumetric/geometric vehicle concept that meets the defined high-level requirements. Within the context of this paper, this is achieved by means of a parametric model. Such parametric models allow varying vehicle configurations, i.e. vehicle parameters, with the aim of examining various design concepts and conducting sensitivity analysis. After evaluating the vehicle concepts, the selected concept establishes the necessary boundary conditions and requirements for the subsequent detailed development process. More precisely, the design process of electrified road vehicles, such as the IUV, involves defining numerous design parameters that are, either directly or indirectly, interconnected. Moreover, vehicle designers must take into consideration multidisciplinary requirements and constraints, such as range, maximum speed, ride comfort, safety, etc. For instance, when targeting a specific driving range, the sizing of the electric drive system is heavily influenced by the vehicle's energy consumption. The electric drive system includes batteries, motors, transmission and, in the case of a fuel cell vehicle, the fuel cell system and hydrogen tanks, whose dimensions should be defined such that the needed energy is supplied. The vehicle's energy consumption, in turn, strongly depends on the total vehicle mass, which is the sum of all vehicle components including the electric drive

system. Moreover, considering the packaging of the electric drive system, it is evident that the vehicle's overall size is strongly dependent on the volume of the individual components, such as the battery. For instance, to cover a higher driving range, a larger battery can be considered to increase the energy supply. Therefore, this increase in the battery volume necessitate an increase in the vehicle's overall size to accommodate these larger components. If, in this case, the vehicle's height is increased, then the aerodynamic drag coefficient changes drastically. Subsequently, the aerodynamic drag coefficient impacts the vehicle's energy consumption and requires adjustments to the sizing of the electric drive system. These interactions between the vehicle parameters are mimicked by the design workflow, which in turn consists of computational tools of each of the engineering disciplines (domains) involved in the conceptual design phase. Table 1) lists the requirements, constraints, design variables and evaluation criteria used for the design workflow of the IUV. Here, it is important to differentiate between design parameters and design variables. Design variables are design parameters that are varied to generate distinct vehicle concepts.

Table 1: IUV's design workflow: high-level multidisciplinary requirements, constraints, design variables and evaluation criteria used in the conceptual design phase of the IUV

Design object	Electrified road vehicle concept
High-level requirements	• Driving performance (acceleration, top speed, range) • Comfort (noise, vibration, harshness, bending and torsional stiffness) • Safety (crash load cases) • Sustainability (sustainable materials, sustainable energy sources)
Constraints	• Max. outer dimensions • Min. interior dimensions • Max. curb weight
Design variables	• Powertrain configuration (e.g. Energy storage ratio battery/hydrogen tank) • Material concept of vehicle structure (body in white)
Evaluation criteria	• Costs (Acquisition Cost, Operating Cost, Total Cost of Ownership) • Energy consumption (Tank-to-wheel, Well-to-wheel)
Workflow builder	MDAx
Workflow executor	RCE

4.3. IUV's simplified design workflow

Within the scope of this paper, the IUV's design workflow, summarized in Table 1, is simplified with the aim of reducing the complexity of the considered system. To be more precise, the constraints, comfort and safety requirements as well as the material and structural concept are not taken into consideration as design variables.
Furthermore, rather than taking all types of costs into account, only the operating costs are used as an evaluation criterion in addition to the energy consumption (see Table 2).

Table 2: IUV's simplified design workflow: high-level multidisciplinary requirements, constraints, design variables and evaluation criteria used in the conceptual design phase of the IUV

Design object	Electrified road vehicle concept			
High-level requirements	**Name**	**Symbol**	**Value**	**Unit**
	Acceleration time from 0 to 100 km/h	t_{0-100}	8.4	s
	Top speed	$v_{\max}$	180	km/h
	Cruise speed	v_{cont}	160	km/h
	Range	R	1000	km
Constraints		–		
Design variables	**Name**	**Symbol**	**Distribution**	**Unit**
	Energy storage ratio	x	$\mathcal{U}[0.1,0.9]$	–
	Fuel cell efficiency	η_{fc}	$\mathcal{U}[0.4,0.6]$	–
	Gravimetric energy density of hydrogen including tank	$\rho^{E}_{\text{G,h}_2\text{,tank}}$	$\mathcal{U}[1400,1600]$	Wh/kg
	Gravimetric energy density of battery	$\rho^{E}_{\text{G,batt}}$	$\mathcal{U}[250,300]$	Wh/kg
Evaluation criteria	**Name**	**Symbol**		**Unit**
	Operating cost	C_{op}		€/km
	Tank-to-wheel energy consumption	E^{ttw}		kWh/km
	Well-to-wheel energy consumption	E^{wtw}		kWh/km
Workflow builder	MDAx			
Workflow executor	RCE			

Four design variables are considered for the IUV's simplified design workflow (see Table 2):

- The energy storage ratio $x \in (0,1)$, i.e., the ratio of the energy stored in the battery to that stored in the hydrogen tank is considered as a design variable. If $x = 0$, then the energy is being solely supplied from the hydrogen tank, i.e. the vehicle is a purely hydrogen-powered one. Whereas, $x = 1$ means that the energy is being completely supplied from the battery. Thus, the vehicle is purely an electric one. Varying x allows the vehicle designer to examine various scenarios regarding the IUV's energy mix. For this purpose, x is assigned a uniform PDF $\mathcal{U}[0.1,0.9]$ with a lower bound of 0.1 and an upper bound of 0.9. Since the IUV is a hybrid road vehicle, the extreme cases, i.e. $x = 0$ and $x = 1$ are excluded.

- The fuel cell efficiency η_{fc} is defined as the ratio of electricity generated to the amount of hydrogen used by the fuel cell [3]. η_{fc} strongly depends on the type of fuel cell technology used. Typically, η_{fc} varies between 40% and 60% [27, 35]. In order to account for various fuel cell technologies, η_{fc} is assigned a uniform PDF ranging between 0.4 and 0.6: $\mathcal{U}[0.4,0.6]$.

- $\rho^{E}_{\text{G,h}_2\text{,tank}}$ is the gravimetric energy density of hydrogen including the tank used for storage. In other words, $\rho_{E,\text{h}_2\text{,tank}}$ denotes the amount of energy stored per unit mass of the storage system, i.e., hydrogen and tank. Within the context of this paper, a variation ranging between 1400 and 1600 Wh/kg is considered. For this reason, $\rho^{E}_{\text{G,h}_2\text{,tank}}$ is a assigned a uniform PDF: $\mathcal{U}[1400,1600]$ Wh/kg.

- $\rho^{E}_{\text{G,batt}}$ is the gravimetric energy density of the entire battery pack including casings, cooling systems, etc. Lithium-ion batteries are currently a well-established technology in electrified vehicles [29]. For such battery systems, Thielmann et al. [34] have provided a forecast of $\rho^{E}_{\text{G,batt}}$ for the years 2025 and 2030. Thielmann et al. predicted that $\rho^{E}_{\text{G,batt}}$ can reach approximately 300 Wh/kg by the year 2030. To consider such future developments of

battery energy systems, this forecast is adopted within the scope of this paper. More precisely, $\rho^{E}_{\mathrm{G,batt}}$ is assigned a uniform distribution $\mathcal{U}[250{,}300]$ Wh/kg.

Two main evaluation criteria (output parameters) are used to evaluate the IUV concepts (see Table 2):

- Operating costs C_{op} refers to the costs needed to supply the IUV with energy, i.e., hydrogen and electricity.

- Energy consumption of the IUV is an essential metric for economic and ecological reasons. The energy consumption impacts strongly the operating costs as well as the greenhouse gas emissions. Here, two types of energy consumption are considered:

    - Tank-to-wheel energy consumption E^{ttw} refers to the energy consumed from the time the energy source, in the IUV's case electricity and hydrogen, is loaded to the vehicle until it is converted to set the vehicle in motion.

    - Well-to-wheel E^{wtw} considers on the other hand the energy needed to produce and transport electricity and hydrogen in addition to the energy consumption of the vehicle. In other words, E^{wtw} provides an overview of all energy-consuming processes involved from the energy source (well) to the wheels of the vehicle.

The IUV's simplified design workflow consists of the following engineering disciplines/domains: vehicle performance, engine, fuel cell, mission, energy storage, mass, cost and lastly well-to-wheel energy consumption.

4.4. Disciplines

In general, the computational tool of each discipline can be mathematically represented as follows:

$$\boldsymbol{y}_{\mathrm{discp}} = \boldsymbol{f}_{\mathrm{discp}}(\boldsymbol{d}_{\mathrm{discp}}, \boldsymbol{c}_{\mathrm{discp}}, \boldsymbol{z}_{\mathrm{discp}}). \tag{7}$$

Here, $\boldsymbol{y}_{discp}$ represents the vector containing the outputs computed and $\boldsymbol{f}_{discp}$: $\boldsymbol{d}_{discp}, \boldsymbol{c}_{discp}, \boldsymbol{z}_{discp} \mapsto \boldsymbol{y}_{discp}$ denotes the vector containing the functions executed by the computational tool of the considered discipline. $\boldsymbol{d}_{discp}$ is defined as the vector including the design variables that are used as inputs for the considered computational tool; $\boldsymbol{c}_{discp}$ corresponds to the vector containing the constants that are used as inputs for the considered computational tool. $\boldsymbol{z}_{discp}$ denotes the vector composed of the linking outputs, i.e., the outputs computed by other computational tools but needed as inputs for the considered computational tool.

Vehicle performance

Within the scope of this discipline, the objective is to determine the power needed considering different scenarios: 1) P_{0-100} needed to accelerate the IUV from 0 to 100 km/h within the required time $t_{0-100} = 8.4$ s, 2) $P_{v_{\max}}$ needed to maintain the required maximum speed $v_{\max} = 180$ km/h, 3) $P_{v_{\mathrm{cont}}}$ needed to maintain the required cruise (continuous) speed $v_{\mathrm{cont}} = 160$ km/h and 4) $P_{\max}$ that should be supplied by the vehicle's engine.

Table 3: Vehicle performance - equations

$P_{0-100} = \left(\underbrace{\frac{1}{2}\rho_{\mathrm{air}} c_{\mathrm{d}} A v_{\mathrm{rated}}^2}_{\text{aerodynamic drag force}} + \underbrace{m g c_{\mathrm{r}}}_{\text{rolling force}} + \underbrace{m e_{\mathrm{i}} a_{\max}}_{\text{inertial force}} \right) v_{\mathrm{rated}}$	(8)
$m = m_{\mathrm{cw}} + m_{\mathrm{payload}},$	(9)

$$a_{\max} = k a_{\text{mean}} = k \frac{\Delta v_{0-100}}{t_{0-100}} = k \frac{100\ \text{km/h}}{t_{0-100}}, k > 1 \quad (10)$$

$$e_{\text{i}} = 1 + \frac{J_{\text{pt,red}}}{m r_{\text{dyn}}} \quad (11)$$

$$P_{v_{\text{max/cont}}} = \left(\underbrace{\frac{1}{2} \rho_{\text{air}} c_{\text{d}} A v_{\text{max/cont}}^2}_{\text{aerodynamic drag force}} + \underbrace{m g c_{\text{r}}}_{\text{rolling force}} \right) v_{\text{max/cont}} \quad (12)$$

$$P_{\max} = \max(P_{0-100}, P_{v_{\max}}) \quad (13)$$

In Table 3, ρ_{air} refers to the air density at room temperature; c_d denotes the drag coefficient; c_r represents the rolling resistance coefficient; A is the vehicle's frontal area and v_{rated} denotes the maximum vehicle speed at which the engine is still delivering maximum torque. Additionally, m refers to the vehicle's mass, which is the sum of the vehicle's curb weight m_{cw} and the mass of some payload m_{payload} (see Eq. 9); $a_{\max}$ quantifies the maximum acceleration within the speed range 0 to 100 km/h (see Eq. 10); e_{i} accounts for the contribution of rotating components to the inertial resistance by taking into consideration the powertrain's reduced moment of inertia $J_{\text{pt,red}}$ and the dynamic wheel radius r_{dyn} (see Eq. 11). Lastly, g denotes the Earth's gravity. The function executed by the computational tool of this discipline is denoted by $\boldsymbol{f}_{\text{vp}}$. The outputs, linking outputs, constants and design variables are listed in Table 4.

Table 4: Vehicle performance - outputs, linking outputs, constants and design variables

Vector	Vector components
$\boldsymbol{y}_{\text{vp}}$	$P_{0-100}, a_{\max}, e_{\text{i}}, P_{v_{\max}}, P_{v_{\text{cont}}}, P_{\max}$
$\boldsymbol{z}_{\text{vp}}$	m_{cw}
$\boldsymbol{c}_{\text{vp}}$	$\rho_{\text{air}}, c_{\text{d}}, A, g, c_{\text{r}}, k, t_{0-100}, r_{\text{dyn}}, J_{\text{pt,red}}, v_{\text{rated}}, v_{\max}, v_{\text{cont}}, m_{\text{payload}}$
$\boldsymbol{d}_{\text{vp}}$	$-$

Engine

The sizing of the engine is determined as follows:

Table 5: Engine discipline - equations

$$P_{\text{eng}} = P_{\max} \quad (14)$$

$$m_{\text{eng}} = \frac{P_{\text{eng}}}{\rho_{\text{G,eng}}^P} = \frac{P_{\max}}{\rho_{\text{G,eng}}^P} \quad (15)$$

$$V_{\text{eng}} = \frac{P_{\text{eng}}}{\rho_{\text{V,eng}}^P} = \frac{P_{\max}}{\rho_{\text{V,eng}}^P} \quad (16)$$

In Table 5, the engine's power P_{eng}, mass m_{eng} and volume V_{eng} are determined empirically based on the gravimetric and volumetric power density of the engine, $\rho_{\text{G,eng}}^P$ and $\rho_{\text{V,eng}}^P$, respectively. The function executed by the computational tool of this discipline is denoted by $\boldsymbol{f}_{\text{eng}}$. The outputs, linking outputs, constants and design variables are listed in Table 6.

Table 6: Engine - outputs, linking outputs, constants and design variables

Vector	Vector components
$\boldsymbol{y}_{\text{eng}}$	$P_{\text{eng}}, m_{\text{eng}}, V_{\text{eng}}$
$\boldsymbol{z}_{\text{eng}}$	$P_{\max}$
$\boldsymbol{c}_{\text{eng}}$	$\rho^{P}_{\text{G,eng}}, \rho^{P}_{\text{V,eng}}$
$\boldsymbol{d}_{\text{eng}}$	$-$

Fuel cell

The sizing of the IUV's fuel cell is determined in a similar manner to that of the engine.

Table 7: Fuel cell - equations

$P_{\text{fc}} = P_{v_{\text{cont}}}$	(17)
$m_{\text{fc}} = \frac{P_{\text{fc}}}{\rho^{P}_{\text{G,fc}}} = \frac{P_{v_{\text{cont}}}}{\rho^{P}_{\text{G,fc}}}$	(18)
$V_{\text{fc}} = \frac{P_{\text{fc}}}{\rho^{P}_{\text{V,fc}}} = \frac{P_{v_{\text{cont}}}}{\rho^{P}_{\text{V,fc}}}$	(19)

The fuel cell's power P_{fc}, mass m_{fc} and volume V_{fc} are determined empirically based on the and gravimetric $\rho^{P}_{\text{G,fc}}$ and volumetric power density. Since the fuel cell is used as a secondary energy source and typically not for acceleration, it is assumed that the fuel cell's power should correspond to $P_{v_{\text{cont}}}$ and not $P_{\max}$.
The function executed by the computational tool of this discipline is denoted by $\boldsymbol{f}_{\text{fc}}$. The outputs, linking outputs, constants and design variables are listed in Table 8.

Table 8: Fuel cell - outputs, linking outputs, constants and design variables

Vector	Vector components
$\boldsymbol{y}_{\text{fc}}$	$P_{\text{fc}}, m_{\text{fc}}, V_{\text{fc}}$
$\boldsymbol{z}_{\text{fc}}$	$P_{v_{\text{cont}}}$
$\boldsymbol{c}_{\text{fc}}$	$\rho^{P}_{\text{G,fc}}, \rho^{P}_{\text{V,fc}}$
$\boldsymbol{d}_{\text{fc}}$	$-$

Mission

To compute the IUV's tank-to-wheel energy consumption, a simple model of an electric drive system is considered. For this purpose, the open-source Modelica simulation tool OpenModelica is used. The model aims at computing the IUV's energy consumption for a given driving cycle $\mathcal{C}$. Within the context of this paper, the WLTP driving cycle is used. The model consists mainly of a battery, electric drive and a gear. Here, the electric drive consists of an electrical machine, converter and controller. The electric drive is a map-based one, i.e., its efficiency is defined at different operating points, which are characterized by a torque and rotational speed. Additionally, the braking force as well as the drag force are modeled. For further details regarding the model, it is referred to [19]. One of the limitations of this model is that the fuel cell is not considered as a part of the electric drive system. However, by considering the IUV's mass, the fuel cell is taken indirectly into consideration. The contribution of the fuel cell in regards to the IUV's energy mix impacts the IUV's mass through the design variable x. To compute the IUV's tank-to-wheel energy consumption E^{ttw}, the energy delivered by the battery $E_{\text{batt}}(t)$ is needed. $E_{\text{batt}}(t)$ varies with time t depending on the driving cycle used. Typically, E^{ttw} is given in kWh/km. As a result, the energy needed to cover the required range E_R^{ttw} can be computed.

Table 9: Mission - equations

$E^{\text{ttw}} = \frac{E_{\text{batt}}(t_{\text{f}})}{d_{\mathcal{C}}}$	(20)
$E_R^{ttw} = E^{\text{ttw}} R$	(21)

In Table 9, t_f denotes the final time and $d_{\mathcal{C}}$ represents the distance traveled by the IUV based on the driving cycle $\mathcal{C}$. The function executed by the computational tool of this discipline is denoted by $\boldsymbol{f}_{\text{mission}}$. The outputs, linking outputs, constants and design variables are listed in Table 10.

Table 10: Mission - outputs, linking outputs, constants and design variables

Vector	Vector components
$\boldsymbol{y}_{\text{mission}}$	$E_{\text{batt}}(t_{\text{f}}), E^{\text{ttw}}$
$\boldsymbol{z}_{\text{mission}}$	m_{cw}
$\boldsymbol{c}_{\text{mission}}$	$\rho_{\text{air}}, c_{\text{d}}, A, g, c_{\text{r}}, r_{\text{dyn}}, J_{\text{ed,red}}, m_{\text{payload}}, \mathcal{C}, SOC_{\text{min}}, SOC_{\text{max}}, SOC_{init}, \beta_{\text{batt}}$
$\boldsymbol{d}_{\text{mission}}$	$-$

In Table 10, $J_{\text{ed,red}}$ denotes the electric drive's reduced moment of inertia; SOC_{min}, SOC_{max} and SOC_{init} represent the minimal, maximal and initial state of charge of the battery, respectively; β_{batt} denotes battery's efficiency.

Energy storage

Within the scope of this discipline, the aim is to determine the appropriate sizing, i.e., the mass and volume of the battery (m_{batt} and V_{batt}) and hydrogen tank (m_{tank} and V_{tank}), such that the required range R is covered. Moreover, the contribution of each energy source ($E_{\text{batt}}^{\text{ttw}}$ and $E_{\text{tank}}^{\text{ttw}}$) to the vehicle's energy consumption is computed.

Table 11: Energy storage - equations

$\bar{E}_{\text{batt}} = \frac{E_R^{ttw}}{\beta_{\text{batt}}} x$	(22)	$\bar{E}_{\text{tank}} = \frac{E_R^{ttw}}{\eta_{\text{fc}}}(1-x)$	(23)
$m_{\text{batt}} = \frac{\bar{E}_{\text{batt}}}{\rho^E_{\text{G,batt}}} = \frac{E^{\text{ttw}} R}{\rho^E_{\text{G,batt}} \beta_{\text{batt}}} x$	(24)	$m_{\text{tank}} = \frac{\bar{E}_{\text{tank}}}{\rho^E_{\text{G,h}_2\text{,tank}}} = \frac{E^{\text{ttw}} R}{\rho^E_{\text{G,h}_2\text{,tank}} \eta_{\text{fc}}}(1-x)$	(25)
$V_{\text{batt}} = \frac{\bar{E}_{\text{batt}}}{\rho^E_{\text{V,batt}}} = \frac{E^{\text{ttw}} R}{\rho^E_{\text{V,batt}} \beta_{\text{batt}}} x.$	(26)	$V_{\text{tank}} = \frac{\bar{E}_{\text{tank}}}{\rho^E_{\text{V,h}_2\text{,tank}}} = \frac{E^{\text{ttw}} R}{\rho^E_{\text{V,h}_2\text{,tank}}}(1-x)$	(27)
$E_{\text{batt}}^{\text{ttw}} = \frac{E^{\text{ttw}}}{\beta_{\text{batt}}} x$	(28)	$E_{\text{tank}}^{\text{ttw}} = \frac{E^{\text{ttw}}}{\eta_{\text{fc}}}(1-x)$	(29)

In Table 11, $\rho^E_{\text{G,batt/h}_2\text{,tank}}$ and $\rho^E_{\text{V,batt/h}_2\text{,tank}}$ denote the gravimetric and volumetric energy density of the battery energy system/hydrogen including tank; x denotes the energy storage ratio of battery to hydrogen tank (design variable); η_{fc} and β_{batt} represent the efficiency of the fuel cell and battery, respectively.
The function executed by the computational tool of this discipline is denoted by $\boldsymbol{f}_{\text{es}}$. The outputs, linking outputs, constants and design variables are listed in Table 12.

Table 12: Energy storage - outputs, linking outputs, constants and design variables

Vector	Vector components
$\boldsymbol{y}_{\text{es}}$	$\bar{E}_{\text{batt}}, m_{\text{batt}}, V_{\text{batt}}, E_{\text{batt}}^{\text{ttw}}, \bar{E}_{\text{tank}}, m_{\text{tank}}, V_{\text{tank}}, E_{\text{tank}}^{\text{ttw}}$
$\boldsymbol{z}_{\text{es}}$	E^{ttw}
$\boldsymbol{c}_{\text{es}}$	$\beta_{\text{batt}}, \rho^E_{\text{V,batt}}, \rho^E_{\text{V,h}_2\text{,tank}}, R$
$\boldsymbol{d}_{\text{es}}$	$x, \rho^E_{\text{G,batt}}, \eta_{\text{fc}}, \rho^E_{\text{G,h}_2\text{,tank}}$

Well-to-Wheel

The purpose of this discipline is to compute the well-to-wheel energy consumption of the IUV E^{wtw}. In other words, the energy consumption, from the production of hydrogen and electricity to their usage during driving, is considered.

Table 13: Well-to-wheel - equations

$E^{\mathrm{wtw}} = \frac{E^{\mathrm{ttw}}_{\mathrm{tank}}}{\eta^{wtw}_{\mathrm{h_2}}} + \frac{E^{\mathrm{ttw}}_{\mathrm{batt}}}{\beta^{\mathrm{wtw}}_{\mathrm{el}}}$	(30)
$E^{\mathrm{wtw}} = \frac{E^{\mathrm{ttw}}}{\eta^{\mathrm{wtw}}_{\mathrm{h_2}}\eta_{\mathrm{fc}}}(1-x) + \frac{E^{\mathrm{ttw}}}{\beta^{\mathrm{wtw}}_{\mathrm{el}}\beta_{\mathrm{batt}}}x$	(31)

In Table 13, $\eta^{\mathrm{wtw}}_{\mathrm{h_2}}$ and $\beta^{\mathrm{wtw}}_{\mathrm{el}}$ denote the well-to-wheel efficiency of hydrogen and electricity, respectively.
The function executed by the computational tool of this discipline is denoted by $\boldsymbol{f_{\mathbf{wtw}}}$. The outputs, linking outputs, constants and design variables are listed in Table 14.

Table 14: Well-to-wheel - outputs, linking outputs, constants and design variables

Vector	Vector components
$\boldsymbol{y}_{\mathrm{wtw}}$	E^{wtw}
$\boldsymbol{z}_{\mathrm{wtw}}$	$E^{\mathrm{ttw}}_{\mathrm{tank}}, E^{\mathrm{ttw}}_{\mathrm{batt}}$
$\boldsymbol{c}_{\mathrm{wtw}}$	$\beta^{\mathrm{wtw}}_{\mathrm{el}}, \eta^{\mathrm{wtw}}_{\mathrm{h_2}}, \beta_{\mathrm{batt}}$
$\boldsymbol{d}_{\mathrm{wtw}}$	x, η_{fc}

Mass

Within the scope of this computational tool, the vehicle's curb weight m_{cw} is calculated by simply adding the mass of the vehicle's components as follows:

Table 15: Mass - equations

$m_{\mathrm{cw}} = m_{\mathrm{eng}} + m_{\mathrm{tank}} + m_{\mathrm{fc}} + m_{\mathrm{batt}} + m_{\mathrm{fix}} = \frac{P_{\mathrm{max}}}{\rho^{P}_{\mathrm{G,eng}}} + \frac{E^{\mathrm{ttw}}R}{\rho^{E}_{\mathrm{G,h_2,tank}}\eta_{\mathrm{fc}}}(1-x) + \frac{P_{v_{\mathrm{cont}}}}{\rho^{P}_{\mathrm{G,fc}}} + \frac{E^{\mathrm{ttw}}R}{\rho^{E}_{\mathrm{G,batt}}\beta_{\mathrm{batt}}}x + m_{\mathrm{fix}}$	(32)

To account for masses of remaining vehicle components (body in white, wheels, etc.), which are not considered in the vehicle's curb weight, a fixed mass denoted by m_{fix} is used in Eq. 32.
The function executed by the computational tool of this discipline is denoted by f_{mass}. The outputs, linking outputs, constants and design variables are listed in Table 16.

Table 16: Mass - outputs, linking outputs, constants and design variables

Vector	Vector components
$\boldsymbol{y}_{\mathrm{mass}}$	m_{cw}
$\boldsymbol{z}_{\mathrm{mass}}$	$P_{\mathrm{max}}, P_{v_{\mathrm{cont}}}, E^{\mathrm{ttw}}$
$\boldsymbol{c}_{\mathrm{mass}}$	$\rho^{P}_{\mathrm{G,eng}}, \rho^{P}_{\mathrm{G,fc}}, \beta_{\mathrm{batt}}, m_{\mathrm{fix}}, R$
$\boldsymbol{d}_{\mathrm{mass}}$	$x, \eta_{\mathrm{fc}}, \rho^{E}_{\mathrm{G,h_2,tank}}, \rho^{E}_{\mathrm{G,batt}}$

Cost

Within the context of this paper, the operating costs are computed based on the vehicle's tank-to-wheel energy consumption as well as the electricity and hydrogen prices.

Table 17: Costs - equations

$C_{h_2} = c_{h_2} \frac{E_{\text{tank}}^{\text{ttw}}}{\rho_{\text{G,h}_2}^E} = c_{h_2} \frac{E^{\text{ttw}}}{\rho_{\text{G,h}_2}^E \eta_{\text{fc}}} (1-x)$	(33)
$C_{\text{el}} = c_{el} E_{\text{batt}}^{\text{ttw}} = c_{el} \frac{E^{\text{ttw}}}{\beta_{\text{batt}}} x$	(34)
$C_{\text{op}} = C_{\text{h}_2} + C_{\text{el}} = c_{\text{h}_2} \frac{E^{\text{ttw}}}{\rho_{\text{G,h}_2}^E \eta_{\text{fc}}} (1-x) + c_{\text{el}} \frac{E^{\text{ttw}}}{\beta_{\text{batt}}} x$	(35)

In Table 17, C_{h_2} and C_{el} denote the vehicle's hydrogen costs and electricity costs, respectively. Typically, the costs of hydrogen gas supplied for hydrogen-fueled vehicles in Europe is given in € per unit mass (c_{h_2}), whereas the electricity costs are typically given in € per unit energy and denoted (c_{el}). $\rho_{\text{G,h}_2}^E$ represents the gravimetric energy of hydrogen. The function executed by the computational tool of this discipline is denoted by $\boldsymbol{f}_{\text{c}}$. The outputs, linking outputs, constants and design variables are listed in Table 18.

Table 18: Costs - outputs, linking outputs, constants and design variables

Vector	Vector components
$\boldsymbol{y}_{\text{c}}$	C_{op}
$\boldsymbol{z}_{\text{c}}$	E^{ttw}
$\boldsymbol{c}_{\text{c}}$	$\rho_{\text{G,h}_2}^E, \beta_{\text{batt}}, c_{\text{h}_2}, c_{\text{el}}$
$\boldsymbol{d}_{\text{c}}$	x, η_{fc}

4.5. Numerical implementation

The design variables used in the IUV's simplified design workflow are collected in vector $\boldsymbol{d} = \boldsymbol{d}_{\text{vp}} \cup \boldsymbol{d}_{\text{eng}} \cup \boldsymbol{d}_{\text{fc}} \cup \boldsymbol{d}_{\text{mission}} \cup \boldsymbol{d}_{\text{es}} \cup \boldsymbol{d}_{\text{mass}} \cup \boldsymbol{d}_{\text{c}} = [\eta_{fc},\ \rho_{\text{G,batt}}^E,\ \rho_{\text{G,h}_2\text{,tank}}^E, x] \in \mathbb{R}^{1\times 4}$. Similarly, all of the constants are represented by vector $\boldsymbol{c} = \boldsymbol{c}_{\text{vp}} \cup \boldsymbol{c}_{\text{eng}} \cup \boldsymbol{c}_{\text{fc}} \cup \boldsymbol{c}_{\text{mission}} \cup \boldsymbol{c}_{\text{es}} \cup \boldsymbol{c}_{\text{mass}} \cup \boldsymbol{c}_{\text{c}}$. To conduct the variance-based GSA, N samples of the design variables $\boldsymbol{d}$ are generated based on the PDFs of the design variables (see Table 2). Here, the Sobol' sequence, which is implemented in the Python library SALib [11, 14] (see Section 2.2), is used for sampling. The constants $\boldsymbol{c}$ are replicated N times. The IUV's design workflow is modeled in MDAx and executed in RCE as follows:

$$\boldsymbol{y}_i = \boldsymbol{f}^{\text{RCE}}(\boldsymbol{d}_i, \boldsymbol{c}_i, \boldsymbol{z}_i). \tag{36}$$

Here, $i = \{1,2,\cdots,N\}$ denotes the sample index, where $N = 20480$. $\boldsymbol{y}$ and $\boldsymbol{z}$ denote the vectors containing the outputs and linking outputs computed by the various disciplines, respectively. They are expressed as follows: $\boldsymbol{y} = \boldsymbol{y}_{\text{vp}} \cup \boldsymbol{y}_{\text{eng}} \cup \boldsymbol{y}_{\text{fc}} \cup \boldsymbol{y}_{\text{mission}} \cup \boldsymbol{y}_{\text{es}} \cup \boldsymbol{y}_{\text{mass}} \cup \boldsymbol{y}_{\text{c}}$ and $\boldsymbol{z} = \boldsymbol{z}_{\text{vp}} \cup \boldsymbol{z}_{\text{eng}} \cup \boldsymbol{z}_{\text{fc}} \cup \boldsymbol{z}_{\text{mission}} \cup \boldsymbol{z}_{\text{es}} \cup \boldsymbol{z}_{\text{mass}} \cup \boldsymbol{z}_{\text{c}}$. The function $\boldsymbol{f}^{\text{RCE}}$ encodes the RCE execution of the computational tools. Within the context of this paper, a vehicle concept, denoted by $\mathcal{V}_i$, is defined to be the set of all vehicle parameters as well as the computational tools connecting these parameters together.

$$\mathcal{V}_i = \{\boldsymbol{y}_i, \boldsymbol{d}_i, \boldsymbol{c}_i, \boldsymbol{z}_i, \mathcal{F}\}, \tag{37}$$

where $\mathcal{F} = \{\boldsymbol{f}_{\text{vp}}, \boldsymbol{f}_{\text{eng}}, \boldsymbol{f}_{\text{fc}}, \boldsymbol{f}_{\text{mission}}, \boldsymbol{f}_{\text{es}}, \boldsymbol{f}_{\text{wtw}}, \boldsymbol{f}_{\text{c}}\}$, denotes the set of all computational tools.

The evaluation criteria used for the IUV's simplified design workflow (see Table 2), i.e. the outputs considered for the variance-based GSA are denoted by $\boldsymbol{y}_i^{GSA} \in \mathbb{R}^{N\times 3}$ and expressed as follows:

$$\boldsymbol{y}_i^{GSA} = [E_i^{\mathrm{ttw}}, E_i^{\mathrm{wtw}}, C_{\mathrm{op},i}]. \tag{38}$$

Here, E^{ttw} denotes the tank-to-wheel energy consumption, E^{wtw} represents the well-to-wheel energy consumption and C_{op} denotes the operating costs.

5. Results

After sampling the design variables and executing the IUV's simplified design workflow, the outputs considered for the variance-based GSA $\boldsymbol{y}_i^{GSA}$ (see Eq. 38) are examined. The resulting output's PDFs are illustrated in Figure 4.

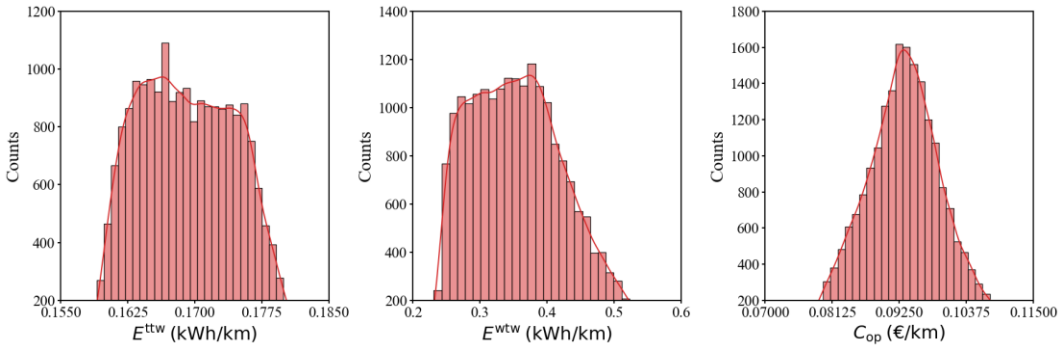

Figure 4: Distribution of the IUV's evaluation criteria (tank-to-wheel energy consumption E^{ttw}, well-to-wheel energy consumption E^{wtw} and operating costs C_{op}). 20480 samples are considered.

The variation of the outputs $\boldsymbol{y}_i^{GSA}$ as a function of the design variables $\boldsymbol{d}_i$ ($i = \{1,2,\cdots,20480\}$) is illustrated in Figure 5.

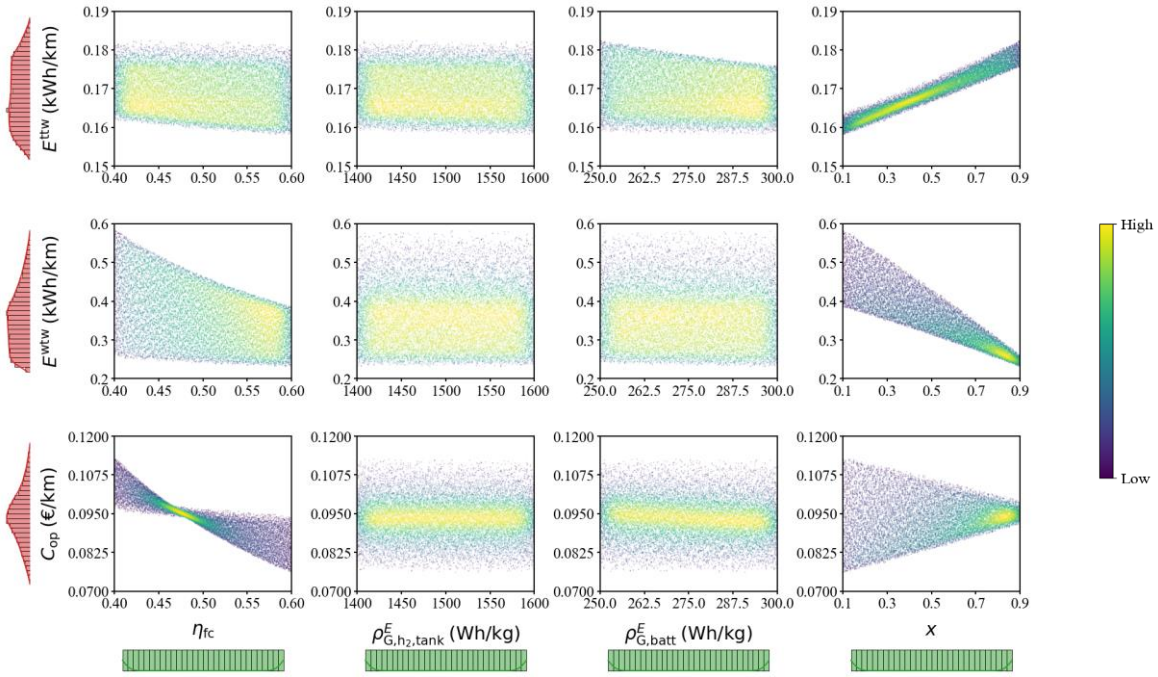

Figure 5: The relation between the outputs (operating costs C_{op}, well-to-wheel energy consumption E^{wtw} and tank-to-wheel energy consumption E^{ttw}) and design variables (fuel cell efficiency η_{fc}, gravimetric energy density of hydrogen including tank $\rho^{E}_{\mathrm{G,h_2,tank}}$, gravimetric energy density of the battery $\rho^{E}_{\mathrm{G,batt}}$ and energy storage ratio x) and their respective PDFs. 20480 samples are considered.

On the vertical and horizontal axis of Figure 5, the outputs and the design variables are plotted with their PDFs, respectively. The colors in the plots encode the density of the outputs in a given region of the design variable. Yellow shaded data points refer to a high-density region, whereas the purple color represents a low-density region. Such scatter plots are useful to recognize some trends and correlations between the design variables and outputs. It is important to mention that observed output fluctuations in the scatter plots, despite the constant value of the design variable on the x-axis, is attributed to the variation in the other design variables that are not held constant. Some key insights can be derived from Figure 5:

- Although the design variables are uniformly distributed, the outputs produced are not uniformly distributed. Such phenomena can be caused by nonlinear relations and the fact that the design variables of the design workflow are interconnected.

- The first column in Figure 5 represents the relation between the fuel cell efficiency η_{fc} and the outputs. It is evident that η_{fc} is strongly correlated to the operating costs C_{op}. More precisely, one observes a decreasing tendency of C_{op}, which agrees well with Eq. 35. Similarly, the well-to-wheel energy consumption E^{wtw} decreases as η_{fc} increases, which also confirms the expected tendency described by Eq. 31. However, comparing the plots of C_{op} and E^{wtw}, it becomes evident that C_{op} has a stronger correlation with η_{fc} and demonstrates a different behavior, especially for $\eta_{\mathrm{fc}} \in [0.45, 0.50]$. Upon analyzing Eq. 31 and 35, one realizes that they share a similar form. Consequently, it is reasonable to anticipate that the outputs E^{wtw} and C_{op} would exhibit comparable behavior; however, this expectation is not fully realized due to the differing coefficients of the summands (see Table 19).

Table 19: Comparison of equations for E^{wtw} and C_{op}

$\boldsymbol{E^{\mathrm{wtw}}}$	$\boldsymbol{C_{\mathrm{op}}}$
$E^{\mathrm{wtw}} = \underbrace{\frac{1}{\eta_{\mathrm{h_2}}^{\mathrm{wtw}}}}_{\text{coeff.}} \frac{E^{\mathrm{ttw}}}{\eta_{\mathrm{fc}}}(1-x) + \underbrace{\frac{1}{\beta_{\mathrm{el}}^{\mathrm{wtw}}\beta_{\mathrm{batt}}}}_{\text{coeff.}} E^{\mathrm{ttw}}x$	$C_{\mathrm{op}} = \underbrace{\frac{c_{h_2}}{\rho_{\mathrm{G,h_2}}^{E}}}_{\text{coeff.}} \frac{E^{\mathrm{ttw}}}{\eta_{\mathrm{fc}}}(1-x) + \underbrace{\frac{c_{el}}{\beta_{\mathrm{el}}^{\mathrm{wtw}}\beta_{\mathrm{batt}}}}_{\text{coeff.}} E^{\mathrm{ttw}}x$

In contrast to E^{wtw} and C_{op}, the tank-to-wheel energy consumption E^{ttw} is poorly correlated to η_{fc}. This can be attributed to the limitation that the mission simulation (see Section 4.4) does not consider the fuel cell to be a part of the electric drive system.

- Examining the second and third columns in Figure 5, it becomes evident that the gravimetric energy densities of hydrogen, including tank, and the battery, $\rho_{\mathrm{G,h_2,tank}}^{E}$ and $\rho_{\mathrm{G,batt}}^{E}$, exhibit a weak correlation with the outputs. Taking a closer look at E^{ttw}, one realizes that correlation between $\rho_{\mathrm{G,batt}}^{E}$ and E^{ttw} is stronger than that of $\rho_{\mathrm{G,h_2,tank}}^{E}$ with E^{ttw}. To get a better understanding of this phenomena, one must examine closely the impact of $\rho_{\mathrm{G,batt}}^{E}$ and $\rho_{\mathrm{G,h_2,tank}}^{E}$ on the vehicle's curb weight m_{cw}, as m_{cw} is an input to the mission simulation, which computes E^{ttw}. Since $\rho_{\mathrm{G,h_2,tank}}^{E} > \rho_{\mathrm{G,batt}}^{E}$, a smaller mass of hydrogen is needed to deliver an equivalent amount of energy compared to the mass of a battery. Therefore, the contribution of $\rho_{\mathrm{G,batt}}^{E}$ to m_{cw} is more impactful than that of $\rho_{\mathrm{G,h_2,tank}}^{E}$, which agrees well with Eq. 32. A visual representation of the relation between the design variables and m_{cw} is illustrated in Figure 6 in a similar manner to Figure 5.

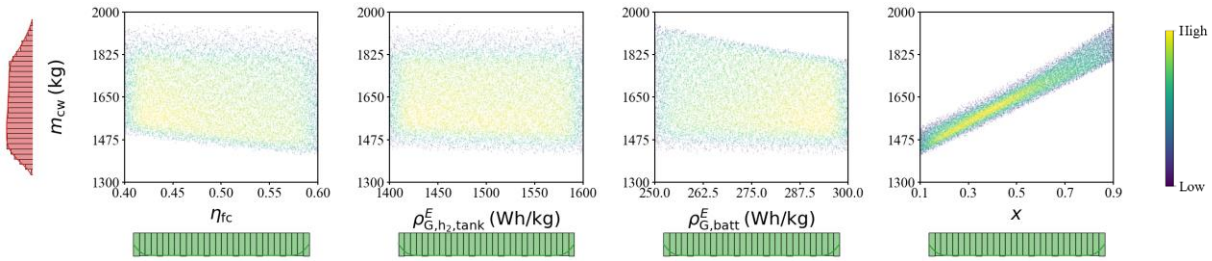

Figure 6: The relation between curb weight m_{cw} and the design variables (fuel cell efficiency η_{fc}, gravimetric energy density of hydrogen including tank $\rho^E_{G,h_2,tank}$, gravimetric energy density of the battery $\rho^E_{G,batt}$ and energy storage ratio x). 20480 samples are considered.

- The last column in Figure 5 illustrates the relation between the energy storage ratio x and the outputs. A strong correlation is seen between the outputs and x. A key observation is the contrasting trends of E^{ttw} and E^{wtw}. As x increases, E^{ttw} exhibits an upward trend, while E^{wtw} demonstrates a downward trend.

E^{ttw}:

To get a better understanding of the E^{ttw} trend, one must examine closely the impact of x on the curb weight m_{cw} (see Figure 6). An increase in x leads to a greater energy extraction from the battery, while reducing the energy drawn from the hydrogen tank. Consequently, this requires an increase in the size of the battery and a reduction in the size of the hydrogen tank, thereby resulting in an increase in the battery's mass m_{batt} and a corresponding decrease in the hydrogen tank's mass m_{tank}. This line of reasoning agrees well with Eq. 24 and 25. From these equations, one can additionally deduce that as x increases, the rate, at which m_{batt} increases, is higher than the rate at which m_{tank} decreases. This is due to the fact that the energy density of hydrogen including tank is higher than that of the battery ($\rho^E_{G,h_2,tank} > \rho^E_{G,batt}$). For this reason, as x increases, the sum of m_{tank} and m_{batt} increases, thus leading to an increase in m_{cw} (see Eq. 32). In other words, the vehicle is heavier, which increases its energy consumption E^{ttw}. Figure 7 illustrates this interplay between m_{tank}, m_{batt} and m_{cw} as a function of x.

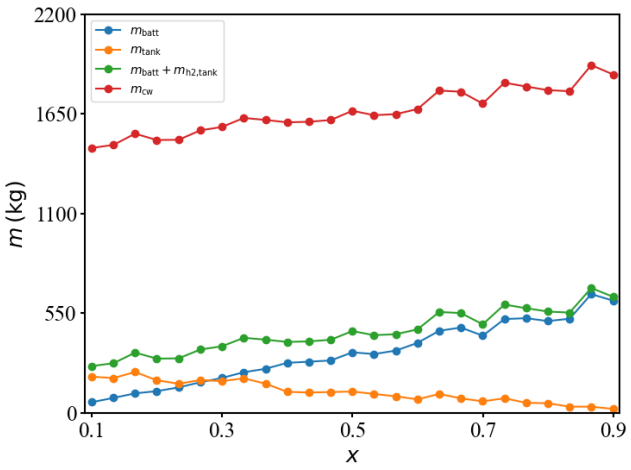

Figure 7: The variation of the battery's mass m_{batt}, the hydrogen tank's mass m_{tank} and the IUV's curb weight m_{cw} as a function of the energy storage ratio x. 25 samples are drawn from 20480 samples.

E^{wtw}:

Intuitively, one expects that E^{wtw} and E^{ttw} would have a similar behavior, since the well-to-wheel energy E^{wtw} accounts for the entire energy lifecycle including the energy consumption during the vehicle's operation E^{ttw}. However, closely examining Eq. 31, it becomes evident that E^{wtw} does not only depend on E^{ttw}, but also on the

infrastructure's efficiency and the efficiency of the vehicle's energy systems, i.e., the well-to-wheel efficiency of hydrogen $\eta_{\mathrm{h_2}}^{\mathrm{wtw}}$, electricity $\beta_{\mathrm{el}}^{\mathrm{wtw}}$, the fuel cell's efficiency η_{fc} and the battery's efficiency β_{batt}. Here, it is assumed that $\beta_{\mathrm{el}}^{\mathrm{wtw}} > \eta_{\mathrm{h_2}}^{\mathrm{wtw}}$ and $\beta_{\mathrm{batt}} > \eta_{\mathrm{fc}}$. In other words, the electric-powered system is more efficient than the hydrogen-fueled one. For this reason, as x increases, the dependency on the electric-powered system increases, thus, resulting in a decrease in E^{wtw}.

Sobol' Indices

In order to quantify the uncertainties of the outputs, i.e. operating costs C_{op}, tank-to-wheel energy consumption E^{ttw} and well-to-wheel energy consumption E^{wtw} caused by the uncertainties of the design variables, i.e. fuel cell efficiency η_{fc}, gravimetric energy densities $\rho^{E}_{\mathrm{G,h_2,tank}}$, $\rho^{E}_{\mathrm{G,batt}}$ and energy storage ratio x, the Sobol' indices come into play. Figure 8 visualizes the notion of the output uncertainties using as an example the relation between the outputs and η_{fc}.

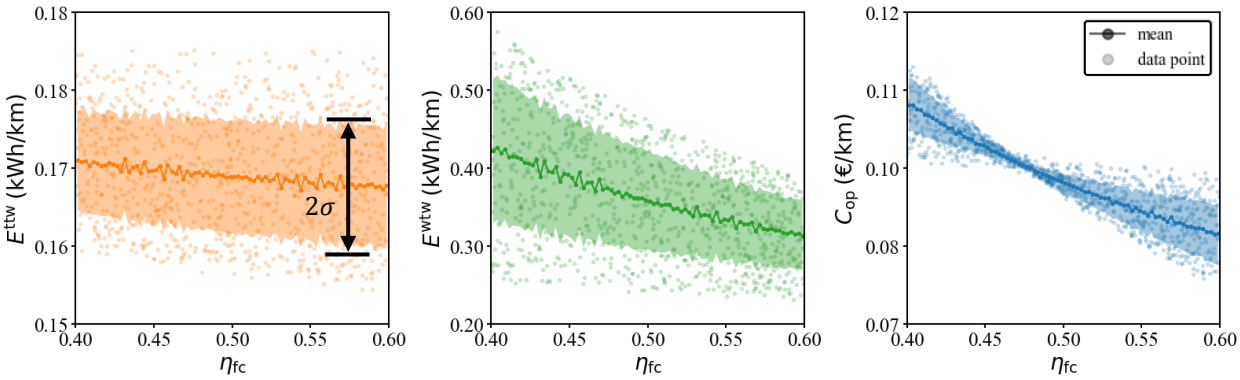

Figure 8: The variation of operating costs C_{op}, tank-to-wheel energy consumption E^{ttw} and well-to-wheel energy consumption E^{wtw} as a function of the design variable fuel cell efficiency η_{fc}. The mean is computed based on 20480 samples. Additionally, 1000 data points are illustrated.

The scattered data points in Figure 8 represent 1000 samples drawn from 20480 samples. Additionally, the mean of each output for a constant η_{fc} is computed over the remaining varying design variables $\rho^{E}_{\mathrm{G,h_2,tank}}$, $\rho^{E}_{\mathrm{G,batt}}$ and x. The shaded area in Figure 8 illustrates the range between the mean plus one standard deviation $\sigma[\cdot]$ and the mean minus one $\sigma[\cdot]$. Since $\sigma[\cdot] = \mathbb{V}[\cdot]^2$ and the variance $\mathbb{V}[\cdot]$ is regarded as a measure for uncertainties within the context of variance-based GSA, the shaded area is considered to be an illustration of the output uncertainties for a constant η_{fc}. However, interesting is the quantification of the output uncertainties considering all design variables:

The uncertainties of which design variables contribute the most to the output uncertainties? In other words, which design variables are the most influential on the outputs?

To answer these questions, the first-order and total Sobol' indices, S_i and $S_{\mathrm{T}i}$, of all outputs are represented in Figure 9. Here, i denotes the index of the design variables η_{fc}, $\rho^{E}_{\mathrm{G},h_2,tank}$, $\rho^{E}_{\mathrm{G},batt}$ and x. It is to be noted that the error bars in Figure 9 represent a confidence level of 95%. In other words, there is a 95% probability that the calculated values of $S_{i/\mathrm{T}i}$ fall within the range indicated by the error bars.

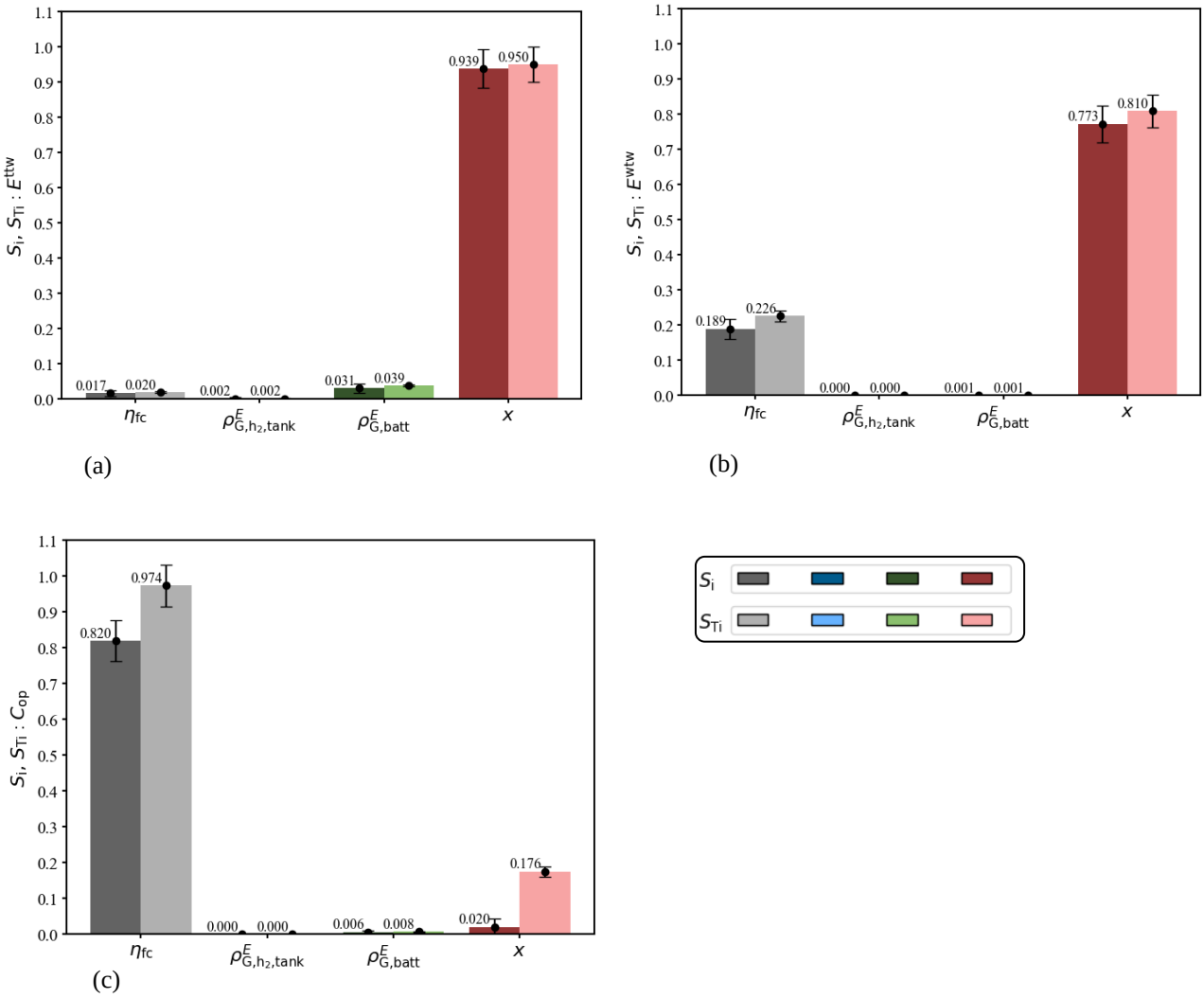

Figure 9: First-order S_i and total order Sobol' indices S_{Ti} of the outputs: tank-to-wheel energy consumption E^{ttw} (a), well-to-wheel energy consumption E^{wtw} (b) and operating costs C_{op} (c).

From Figure 9 (a), it becomes evident that the energy storage ratio x is the most influential design variable with respect to the tank-to-wheel energy consumption E^{ttw}. This agrees well with the scatter plots of E^{ttw} (see Figure 5, upper row). The fact that x exhibits the greatest impact on E^{ttw}, while the effect of the fuel cell efficiency η_{fc} and gravimetric energy densities, $\rho^E_{G,h_2,tank}$ and $\rho^E_{G,batt}$ is minimal, suggests that any technological improvements regarding the fuel cell and battery have a much lower impact on the vehicle's tank-to-wheel energy consumption in comparison to the vehicle's energy storage configuration. However, since within the mission simulation (see Section 4.4) the fuel cell was not modelled, an extension of the simulation is required to get more accurate results regarding the impact of the fuel cell efficiency on the tank-to-wheel energy consumption. Moreover, since $S_i - S_{Ti} \approx 0$, one can assume that the interaction between the design variables, η_{fc}, $\rho^E_{G,h_2,tank}$, $\rho^E_{G,batt}$ and x, has a negligible effect on the sensitivity of E^{ttw}.

Taking a closer look at Figure 9 (b), one realizes that the impact of the gravimetric energy densities, $\rho^E_{G,h_2,tank}$ and $\rho^E_{G,batt}$, on the well-to-wheel energy consumption E^{wtw} is negligible. The most impactful design variables are the energy storage ratio x followed by the fuel cell efficiency η_{fc}. This indicates that although x exhibits the dominant influence on the sensitivity of E^{wtw}, improvements in η_{fc} can reduce E^{wtw}. What is particularly evident is the slight difference between S_i and S_{Ti} for both x and η_{fc}, which implies that there exists an interaction between x and η_{fc}. This interplay, which affects the sensitivity of E^{wtw}, aligns well with Eq. 31, which shows that x and η_{fc} influence

simultaneously the first summand of E^{wtw}. To get a better understanding of this interplay and its impact on E^{wtw}, Figure 10 illustrates E^{wtw} as a function of x and η_{fc}. The colors in Figure 10 (a) and (b) represent the variation of x and η_{fc}, respectively. Examining Figure 10 (a), it becomes evident that for small values of x (blue dots, $x < 0.5$) the impact of η_{fc} on E^{wtw} is bigger. In other words, the rate at which E^{wtw} decreases, as η_{fc} increases, is bigger for small x values. This is due to the fact that, for small x values, the vehicle's reliance on the hydrogen-powered system is greater. Thus, the impact of the fuel cell becomes greater. Shifting the attention to Figure 10 (b), one can deduce that for small η_{fc} values (blue dots, $\eta_{\mathrm{fc}} < 0.5$), E^{wtw} is greater, which is consistent with intuitive expectations. Moreover, for all η_{fc} values, as x increases, E^{wtw} tend to converge to a single value region. This is attributed to the increase in the vehicle's reliance on the electric system. Thus, the impact of the fuel cell becomes smaller.

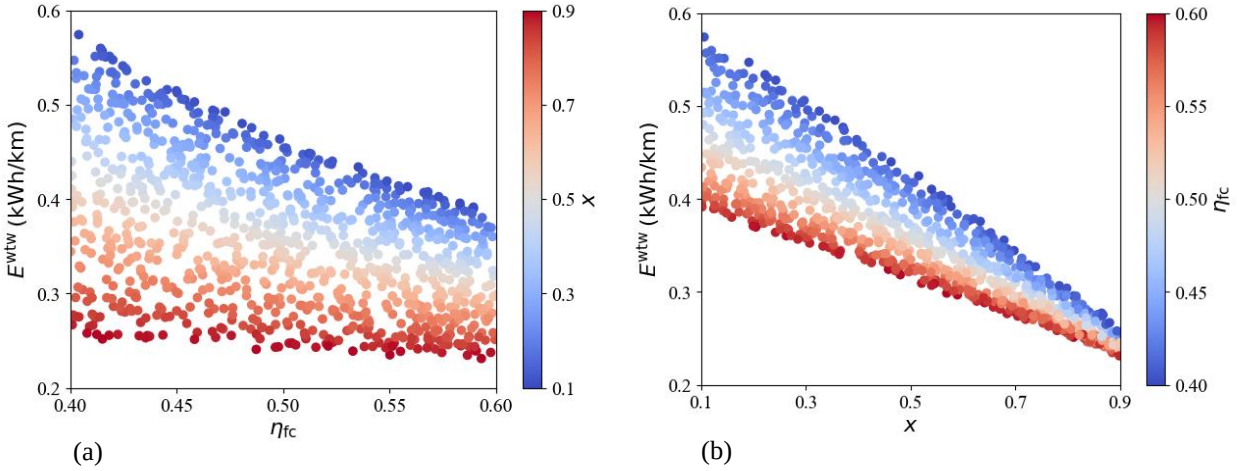

Figure 10: The variation of the well-to-wheel energy consumption E^{wtw} as a function of fuel cell efficiency η_{fc} and the energy storage ratio x. 1000 samples are drawn from 20480 samples.

Figure 9 (c) shows as well no significant impact of the gravimetric energy densities, $\rho^{E}_{\mathrm{G,h_2,tank}}$ and $\rho^{E}_{\mathrm{G,batt}}$, on the operating costs C_{op}. In contrast to E^{wtw}, the most influential design variable with respect to C_{op} is the fuel cell efficiency η_{fc} followed by the energy storage ratio x. A key observation is that for x, $S_{\mathrm{T}i} \gg S_i$ and $S_i \approx 0$.
The fact that $S_i \approx 0$ indicates that x does not directly impact C_{op}. Moreover, since $S_{\mathrm{T}i} \gg S_i$, one deduces that x influences C_{op} indirectly. More precisely, x impacts C_{op} through its interaction, particularly with the fuel cell efficiency η_{fc} since $S_i - S_{\mathrm{T}i} \neq 0$, for both x and η_{fc}. To gain a deeper insight into the interaction between x and η_{fc} and their impact on C_{op}, Figure 11 (a) and (b) represent C_{op} as a function of η_{fc} and x, respectively. From Figure 11 (a) it becomes evident, the impact of η_{fc} on C_{op} diminishes for high x values (red dots), which is as well attributed to the increase in the vehicle's reliance on the electric system. Thus, the impact of η_{fc} becomes smaller. Additionally, Figure 11 (b) shows that to understand the relation between C_{op} and x, the values of η_{fc} should be taken into consideration as well. As x increases, C_{op} increases for high η_{fc} values (red dots, $\eta_{\mathrm{fc}} > 0.5$), while C_{op} decreases for low η_{fc} values (blue dots, $\eta_{\mathrm{fc}} < 0.5$).

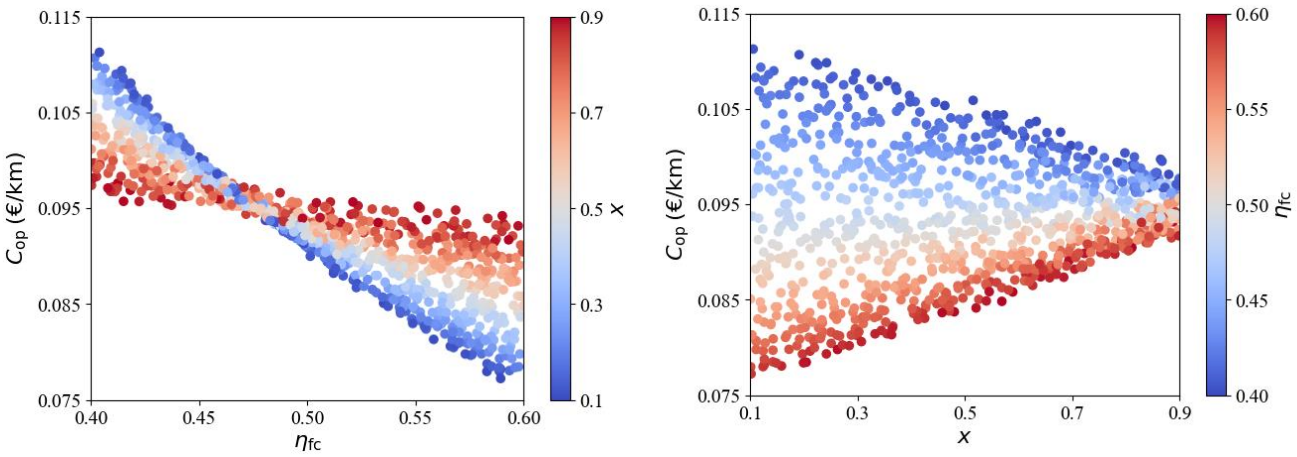

Figure 11: The variation of the well-to-wheel energy consumption C_{op} as a function of fuel cell efficiency η_{fc} and the energy storage ratio x. 1000 samples are drawn from 20480 samples.

6. Summary and Outlook

Within the context of this paper, a framework was provided to integrate a variance-based global sensitivity analysis (GSA) in the multidisciplinary conceptual phase of road vehicles. To ensure the applicability of this framework, the conceptual design phase of the so called "Inter-urban vehicle" (IUV) was examined. The IUV is a research plug in fuel cell electric vehicle, which is conceptualized at German Aerospace Centre (DLR[5]). With the aim of digitizing and automating the conceptual design phase, a digital vehicle design workflow was modeled using the multidisciplinary design analysis and optimization workflow design accelerator, abbreviated as MDAx. To guarantee an efficient exchange of computational tools between the engineering teams involved in the conceptual phase, the vehicle design workflow was executed in the open-source software RCE, short for **r**emote **c**omponent **e**nvironment. Within the context of this paper, the energy storage ratio x, fuel cell efficiency η_{fc} and the gravimetric energy densities of the battery as well as hydrogen including tank, $\rho^{E}_{\mathrm{G,batt}}$ and $\rho^{E}_{\mathrm{G,h_2,tank}}$, were regarded as design variables. The uncertainties of the design variables, which can be due to future technological advancements or different vehicle configurations, were quantified using probability distribution functions (PDF). Based on these PDFs, the design variables were sampled using the Sobol' sequence. Subsequently, the resulting design workflows were executed in the process-integrating software RCE. Here, the tank-to-wheel E^{ttw} and well-to-tank energy consumption E^{wtw} as well as the operating costs C_{op} were considered as quantities of interest (outputs) for the subsequent GSA, where the Sobol' indices of the outputs were computed based on the Sobol' method. It was shown that the Sobol' indices did not only quantify the uncertainties of the outputs, but also helped to identify which design factors are the most influential on the final vehicle design. Additionally, Sobol' indices helped in comprehending the intricate mechanisms of the system under consideration, which facilitates the decision-making process in the conceptual design phase of road vehicles.

An important factor that was not considered in this paper is the computational time. Since the Sobol' method require a large number of samples to achieve an acceptable accuracy, a high computational effort was needed to evaluate the IUV's design workflows. For this reason, further investigations can be conducted with the objective of applying surrogate models, that can replace the IUV's design workflow while reducing the computational effort required.
What was also not considered in this paper, are uncertainties related to the computational tools used for the design workflow, such as, uncertainties due to numerical errors. Within the context of upcoming work, the framework presented in this paper can be extended to include such uncertainties. Future research could also include extending the

[5] DLR: Deutsches Zentrum für Luft- und Raumfahrt

IUV's design workflow to account for additional engineering domains, which are involved in the conceptual design phase, such as aerodynamics, lateral dynamics, packaging, etc.
Finally, different methods could be investigated in future work with the aim of evaluating the large number of vehicle concepts resulting from sampling. Subsequently, the values of the design variables yielding to the optimal vehicle concept can be selected based on the evaluation method chosen.

Acknowledgements

This research was supported by the German Aerospace Center in Stuttgart, Germany. We thank Mr. Sebastian Vohrer for providing the Python code used within the context of this paper. We also appreciate the resources provided by the Institute of Vehicle Concepts at the German Aerospace Center.

References

[1] Marko Alder, Erwin Moerland, Jonas Jepsen, and Björn Nagel. 2020. Recent Advances in Establishing a Common Language for Aircraft Design with CPACS. *Aerospace Europe Conference 2020, Bordeaux*.

[2] Jong-Jin Bae and Namcheol Kang. 2018. Development of a Five-Degree-of-Freedom Seated Human Model and Parametric Studies for Its Vibrational Characteristics. *Shock and Vibration* 2018, 1–15. DOI: https://doi.org/10.1155/2018/1649180.

[3] Frano Barbir. 2013. *PEM fuel cells*: *Theory and practice*. Elsevier, Amsterdam, Boston, Heidelberg, London, New York, Oxford, Paris, San Diego, San Francisco, Singapore, Sydney, Tokyo.

[4] Brigitte Boden, Jan Flink, Niklas Först, Robert Mischke, Kathrin Schaffert, Alexander Weinert, Annika Wohlan, and Andreas Schreiber. 2021. RCE: An Integration Environment for Engineering and Science. *SoftwareX* 15, 100759. DOI: https://doi.org/10.1016/j.softx.2021.100759.

[5] B. Boutra, A. Sebti, and M. Trari. 2022. Response surface methodology and artificial neural network for optimization and modeling the photodegradation of organic pollutants in water. *Int. J. Environ. Sci. Technol.* 19, 11, 11263–11278. DOI: https://doi.org/10.1007/s13762-021-03875-1.

[6] Adam Brandt, Bengt Jacobson, and Simone Sebben. 2022. High speed driving stability of road vehicles under crosswinds: an aerodynamic and vehicle dynamic parametric sensitivity analysis. *Vehicle System Dynamics* 60, 7, 2334–2357. DOI: https://doi.org/10.1080/00423114.2021.1903516.

[7] B. Danquah, A. Koch, A. Pinnel, T. Weiß, and M. Lienkamp. 2019. *Component Library for Entire Vehicle Simulations*.

[8] Benedikt Danquah, Stefan Riedmaier, Yasin Meral, and Markus Lienkamp. 2021. Statistical Validation Framework for Automotive Vehicle Simulations Using Uncertainty Learning. *Applied Sciences* 11, 5, 1983. DOI: https://doi.org/10.3390/app11051983.

[9] Armen Der Kiureghian and Ove Ditlevsen. 2009. Aleatory or epistemic? Does it matter? *Structural Safety* 31, 2, 105–112. DOI: https://doi.org/10.1016/j.strusafe.2008.06.020.

[10] Roger Ghanem, David Higdon, and Houman Owhadi, Eds. 2017. *Handbook of uncertainty quantification*. Springer Reference. Springer Nature, Cham, Switzerland. DOI: https://doi.org/10.1007/978-3-319-12385-1.

[11] Herman, J., and Usher, W. *SALib.sample.saltelli module* (accessed 01-August-2024). Retrieved from https://salib.readthedocs.io/en/latest/api/SALib.sample.html.

[12] Homma, Toschimitsu and Saltelli Andrea. 1996. Importance measures in global sensitivity analysis of nonlinear models. *Reliability Engineering & System Safety*, 1–17.

[13] Eyke Hüllermeier and Willem Waegeman. 2021. Aleatoric and epistemic uncertainty in machine learning: an introduction to concepts and methods. *Mach Learn* 110, 3, 457–506. DOI: https://doi.org/10.1007/s10994-021-05946-3.

[14] Takuya Iwanaga, William Usher, and Jonathan Herman. 2022. Toward SALib 2.0: Advancing the accessibility and interpretability of global sensitivity analyses. *SESMO* 4, 18155. DOI: https://doi.org/10.18174/sesmo.18155.

[15] Zhen Jiang, Wei Chen, and Brian J. German. 2016. Multidisciplinary Statistical Sensitivity Analysis Considering Both Aleatory and Epistemic Uncertainties. *AIAA Journal* 54, 4, 1326–1338. DOI: https://doi.org/10.2514/1.J054464.

[16] Marc C. Kennedy and Anthony O'Hagan. 2001. Bayesian calibration of computer models. *Journal of the Royal Statistical Society: Series B (Statistical Methodology)* 63, 3, 425–464. DOI: https://doi.org/10.1111/1467-9868.00294.

[17] Andrew B. Lambe and Joaquim R. R. A. Martins. 2012. Extensions to the design structure matrix for the description of multidisciplinary design, analysis, and optimization processes. *Struct Multidisc Optim* 46, 2, 273–284. DOI: https://doi.org/10.1007/s00158-012-0763-y.

[18] M. Alder, B. Fröhler, T. Ahmed, A. Skopnik. 2023. Assessment of Techniques for Global Sensitivity Analyses in Conceptual Aircraft Design. *AIAA AVIATION 2023 Forum*.

[19] Massimo Ceraolo. 2017. Simplified Modelling of Electric and Hybrid Vehicles.

[20] Marco Münster. 2020. Vorgehensmodell zur Grundkonzeption eines Fahrzeugkonzepts und Entwicklung neuartiger kraftflussoptimierter Karosseriestrukturen für elektrifizierte Fahrzeuge (Procedure model for the basic conception of vehicle concepts and development of new body structures optimized for electrified vehicles). *DLR Forschungsbereicht*.

[21] Nicolae Dăneț. 2007. Interval Analysis A Powerful Trend in Numerical Analysis. *International Conference: Trends and Challenges in Applied Mathematics*.

[22] Efstratios Nikolaidis, Dan M. Ghiocel, and Suren Singhal. 2008. *Engineering design reliability applications*: *For the aerospace, automotive, and ship industries*. CRC Press, Boca Raton.

[23] A. Page Risueño, J. H. Bussemaker, P. D. Ciampa, and B. Nagel. 2020. MDAx: Agile Generation of Collaborative MDAO Workflows. *AIAA AVIATION 2020 Forum*.

[24] Patrick M. Reed, Antonia Hadjimichael, Keyvan Malek, Tina Karimi, Chris R. Vernon, Vivek Srikrishnan, Rohini S. Gupta, David F. Gold, Ben Lee, Klaus Keller, Travis B. Thurber, Jennie S. Rice. 2022. *Addressing Uncertainty in MultiSector Dynamics Research* (2022). Retrieved from https://uc-ebook.org/docs/html/ acknowledgements.html.

[25] Saman Razavi, Anthony Jakeman, Andrea Saltelli, Clémentine Prieur, Bertrand Iooss, Emanuele Borgonovo, Elmar Plischke, Samuele Lo Piano, Takuya Iwanaga, William Becker, Stefano Tarantola, Joseph H. Guillaume, John Jakeman, Hoshin Gupta, Nicola Melillo, Giovanni Rabitti, Vincent Chabridon, Qingyun Duan, Xifu Sun, Stefán Smith, Razi Sheikholeslami, Nasim Hosseini, Masoud Asadzadeh, Arnald Puy, Sergei Kucherenko, and Holger R. Maier. 2021. The Future of Sensitivity Analysis: An essential discipline for systems modeling and

policy support. *Environmental Modelling & Software* 137, 104954. DOI: https://doi.org/10.1016/j.envsoft.2020.104954.

[26] Andrea Saltelli. 2002. Making best use of model evaluations to compute sensitivity indices. *Computer Physics Communications* 145, 2, 280–297. DOI: https://doi.org/10.1016/S0010-4655(02)00280-1.

[27] Norazlianie Sazali, Wan N. Wan Salleh, Ahmad S. Jamaludin, and Mohd N. Mhd Razali. 2020. New Perspectives on Fuel Cell Technology: A Brief Review. *Membranes* 10, 5. DOI: https://doi.org/10.3390/membranes10050099.

[28] Simon Schmeiler. 2016. Application of stochastic modeling and simulation to vehicle system dynamics. *7th International Munich Chassis Symposium 2016*, 227–260. DOI: https://doi.org/10.1007/978-3-658-14219-3_19.

[29] Richard Schmuch, Ralf Wagner, Gerhard Hörpel, Tobias Placke, and Martin Winter. 2018. Performance and cost of materials for lithium-based rechargeable automotive batteries. *Nat Energy* 3, 4, 267–278. DOI: https://doi.org/10.1038/s41560-018-0107-2.

[30] Dieter Schramm, Manfred Hiller, and Roberto Bardini. 2016. *Vehicle Dynamics: Modeling and Simulation*. Springer.

[31] I. M. Sobol'. 1993. Sensitivity Estimates for Nonlinear Mathematical Models. *MMCE*.

[32] Byoung-Gyu Song, Jong-Jin Bae, and Namcheol Kang. 2023. Uncertainty Quantification of Ride Comfort Based on gPC Framework for a Fully Coupled Human–Vehicle Model. *Applied Sciences* 13, 11, 6785. DOI: https://doi.org/10.3390/app13116785.

[33] Bruno Sudret. 2008. Global sensitivity analysis using polynomial chaos expansions. *Reliability Engineering & System Safety* 93, 7, 964–979. DOI: https://doi.org/10.1016/j.ress.2007.04.002.

[34] A. Thielmann, C. Neef, T. Hettesheimer, H. Döscher, M. Wietschel, and J. Tübke. 2017. Energiespeicher-Roadmap (Update 2017): Hochenergie-Batterien 2030+ und Perspektiven Zukünftiger Batterietechnologien.

[35] U.S. Departement of Energy. 2015. *Fuel Cell Technologies Office* (2015). Retrieved from https:// www.energy.gov/eere/fuelcells/articles/fuel-cells-fact-sheet.

[36] Norbert Wiener. 1938. The Homogeneous Chaos. *American Journal of Mathematics* 60, 4, 897. DOI: https://doi.org/10.2307/2371268.

[37] Jinglai Wu, Zhen Luo, Nong Zhang, and Yunqing Zhang. 2015. A new uncertain analysis method and its application in vehicle dynamics. *Mechanical Systems and Signal Processing* 50-51, 659–675. DOI: https://doi.org/10.1016/j.ymssp.2014.05.036.